BIOCHEMISTRY
including biophysical chemistry & molecular biology
Article

Biochemistry **2010,** *49,* 8043–8052 8043
DOI: 10.1021/bi100663u

Multiconformation Continuum Electrostatics Analysis of the Effects of a Buried Asp Introduced near Heme *a* in *Rhodobacter sphaeroides* Cytochrome *c* Oxidase[†]

Jun Zhang and M. R. Gunner*

Physics Department, J-419, City College of New York, 160 Convent Avenue, New York, New York 10031

Received April 29, 2010; Revised Manuscript Received August 11, 2010

ABSTRACT: Cytochrome *c* oxidase (CcO) reduces O_2 to water via a series of proton-coupled electron transfers, generating a transmembrane electrochemical gradient. Coupling electron and proton transfer requires changing the pK_a values of buried residues at each stage in the reaction cycle. Heme *a* is a key cofactor in the CcO electron transfer chain. Mutation of Ser44 to Asp has been reported [Mills, D. A., et al. (2008) *Biochemistry 47*, 11499−11509], changing the hydrogen bond acceptor from His102, the heme *a* axial ligand in *Rhodobactor sphaeroides* CcO. This adds an acidic residue to the CcO interior. The electrochemical behavior of heme *a* in wild-type and S44D CcO is compared using the continuum electrostatics program MCCE. The introduced, deeply buried Asp remains ionized at physiological pH only when the nearby heme is oxidized. Heme *a* reduction is now calculated to be strongly coupled to Asp proton binding, while with Ser44, it is weakly coupled to small protonation shifts at multiple sites, increasing the pH dependence in the mutant. At pH 7, the partially ionized Asp 44 is calculated to lower the heme redox potential by 50 mV as expected given the thermodynamics of coupled electron and proton transfers. This highlights an curious finding in the experimental results where a low Asp pK_a is found together with a stabilized reduced heme. The stabilization of a heme oxidation in a model complex by a hydrogen bond to the axial His ligand calculated with continuum electrostatics and with density functional theory were in good agreement.

Cytochrome *c* oxidase (CcO)[1] is the terminal protein of the aerobic respiratory chain in plants, animals, and many bacteria. There are four redox centers within the protein: Cu_A, heme *a*, Cu_B, and heme a_3. Electrons are sequentially transferred from cytochrome *c* to Cu_A, to heme *a*, and then to the binuclear center composed of Cu_B and heme a_3, where an oxygen molecule is reduced to water. Like other intrinsic membrane electron transfer proteins, CcO strongly influences the free energy of ionization of the deeply buried sites within the protein (*1*, *2*). The electron transfers between the redox sites than lead to changes in the pK_a values of the surrounding groups, thus changing protonation states of appropriate residues at each stage of the reaction cycle (*3*, *4*). It is these coupled reactions that allow the electron transfer reactions to drive transmembrane proton transfer (*4*, *5*). In CcO, synchronized with the four-electron transfers needed to form water, eight protons are removed from the cell interior. Four are transported to the binuclear center for addition to the substrate oxygen, while the other four are pumped to the outer side of the membrane, adding to the electrochemical proton gradient across the membrane (*6*−*8*).

Heme *a*, the focus of the work reported here, is an *a*-type, low-spin heme with two axial histidine ligands (*9*). A nonredundant survey of 132 *b*- and *c*-type hemes (*10*) has shown that with a His axial ligand, 75% of the distal His nitrogens (those not involved in ligation to the heme iron) make a hydrogen bond to the protein. Of these, 40% are to a backbone carbonyl and 3.2% are to the side chain of Ser as found for heme *a* in *Rhodobacter sphaeroides* CcO. Asp, which will be introduced as a hydrogen bond acceptor in the work presented here, is found 9.5% of the time. In CcO, heme a_3 has a single His ligand, leaving a site free to bind oxygen for reduction to water. His 419, the heme a_3 ligand, makes a hydrogen bond to Gly 294, the heme *a* ligand, His 421 a hydrogen bond to the Val 417 backbone carbonyl, and His 102 a hydrogen bond to the side chain of Ser44 (*Rb. sphaeroides* residue numbering). An HSSP analysis of 2264 oxidase analogues with as little as 32% percent identity and 46% percent similarity (*11*) shows the backbone Gly and Val hydrogen bonds associated with the heme a_3 and *a* ligands are 100% conserved. In contrast, a Ser hydrogen bond is found in only 6% of the oxidases, 93% of the sequences have a Gly in this position, and 1% have Ala. In the bovine crystal structure, Gly 30 (bovine numbering), aligned with Ser 44 in the sequence, is the hydrogen bond acceptor from the His 61 ligand to heme *a*. However, sequence alignment does not always result in structural conservation. For example, the *Paracoccus denitrificans* structure [Protein Data Bank (PDB) entry 3HB3] has Ser 46 in the aligned sequence, but the side chain of Thr 50 is in a better position to form a hydrogen bond to the His ligand of heme *a*.

Recent studies have reported on the changes in the electron transfer reactions when the Ser hydrogen bond donor to the heme *a* axial ligand is replaced with Gly, Asn, or Asp in *Rb. sphaeroides* CcO (*12*). Visible and EPR spectroscopy and X-ray crystallography show that the structure of the protein is not significantly perturbed by the mutations. The rate of transfer of electrons from Cu_A to heme *a* has been measured by a light-activated ruthenium donor (*13*, *14*). At pH 7−8 in wild-type oxidase, the transfer of electrons from Cu_A to heme *a* occurs at rates from 2×10^4 s^{-1} in bovine (*13*) or *P. denitrificans* (*15*) to 9×10^4 in *Rb.*

[†]This work was supported by National Institutes of Health (NIH) Grant 1R01GM084028-01A2, with infrastructure support from NIH Grant 5G12 RR03060.

*To whom correspondence should be addressed. Telephone: (212) 650-5557. Fax: (212) 650-6940. E-mail: gunner@sci.ccny.cuny.edu.

[1]Abbreviations: CcO, cytochrome *c* oxidase; MCCE, Multi-Conformer Continuum Electrostatics, rmsd, root-mean-square deviation.

Published on Web 08/11/2010

Table 1: Definitions of Structures[a]

designation	comments	length of the H-bond to H102 (Å)[b]	rmsd for 2GSM (Å)[c]
WT_S44	Protein Data Bank entry 2GSM	2.85	0
WT*_D44	MCCE mutates D44 to S44 in WT_S44 (2GSM) followed by GROMACS relaxation	3.10	0.14
WT*_S44	MCCE mutates D44 to S44 in WT*_D44	3.58	0.14
MUT_D44	S44D X-ray structure; 12 surface residues labeled Ala	2.71	0.37
MUT*_D44	GROMAC relaxation of MUT_D44	2.88	0.44
MUT*_S44	MCCE mutates D44 to S44 in MUT*_D44	3.60	0.44
MUT*_D44#	MCCE replaces surface Ala with wild-type residues in MUT*_D44	2.86	0.44
MUT*_S44#	MCCE replaces surface Ala with wild-type residues in MUT*_S44	3.69	0.44

[a]Abbreviations: WT, structure derived from PDB entry 2GSM; MUT, structure derived from the X-ray crystal structure from S. Ferguson-Miller of the D44S mutant with 12 surface residues designated as Ala. GROMACS optimization conducted with ionized Asp at position 44 once for each parent structure. Relaxation of the other structures was conducted with MCCE optimization of side chain packing. Asterisks identify structures minimized using GROMACS. Number signs identify samples in which 12 unresolved side chains in the MUT_ structure reverted to the 2GSM wild-type sequence. [b]Distance from the side chain oxygen of Ser or Asp 44 to the Nε proton of His 102. [c]The rmsd of the backbone atoms.

sphaeroides (*14*) CcO. A reaction free energy difference of 40−50 meV is derived from the observation that 12−18% of the electrons remain on Cu_A rather than proceeding to heme *a*. The rate of transfer of electrons from Cu_A to heme *a* in the Asn and Gly mutant remains faster than the rate of transfer of electrons from cytochrome *c* to Cu_A ($\approx 7 \times 10^4$ s^{-1}). However, with Asp 44, reduction of heme *a* occurs at a rate of ≈ 125 s^{-1} at pH 8. Now as the pH is lowered, a second, fast phase of electron transfer is found, which is indistinguishable from that of the wild-type protein in these experiments ($> 3 \times 10^4$ s^{-1}). These results support a model in which the fast, low-pH rate occurs in the presence of a protonated Asp 44 (*12*). As the pH is increased when heme *a* is oxidized, the Asp is deprotonated. However, heme *a* reduction slows as it is now tightly coupled to proton binding by the Asp. The fast and slow phases have equal amplitudes near pH 5.5, the apparent pK_a of Asp 44. In addition, at pH > 6.5, reduction of heme *a* by Cu_A is now favored by at least 60 meV, as no reduced Cu_A is seen at equilibrium (*12*).

The results suggest that an Asp placed in a deeply buried site in the transmembrane cytochrome *c* oxidase has a pK_a of ≈ 5.5, only 1.8 pH units higher than that of an Asp in solution. The energy penalty for removing the ionized form of a residue from water is more significant than for the neutral form, shifting the equilibrium constant to favor charge neutralization (*16*−*18*). Thus, surveys show that most acidic and basic amino acids are on the surface of the protein (*19*). However, a significant minority is in fact buried, and these often represent residues that are important for enzyme function (*20*). Buried, native amino acids exist in locations that are optimized by evolution. Calculations of the buried acidic and basic residues in 500 proteins suggest that they remain ionized at physiological pH because of interactions with the backbone dipoles and other amino acid side chains (*19*). The Asp 44 that was introduced into CcO represents a charge introduced into a naive site. A recent study introduced Asp, Arg, Glu, and Lys into 25 sites in the hydrophobic interior of *Staphylococcus* nuclease and six sites in ribonuclease H (*21*). With few exceptions, the introduced acid or base has a pK_a greatly shifted to favor the neutral form. In addition, when this new residue is charged, the protein is often significantly destabilized. It is thus of interest to understand how CcO is able to accommodate this new charge at Asp 44.

Cytochrome *c* oxidase has been the subject of extensive computational studies with a wide variety of methods. Recent studies have employed QM/MM to study the energetics of oxygen reduction (*22*). The role of key amino acids for controlling proton pumping has been studied by QM/MM (*23*), empirical valence bond molecular dynamics (*24*), dynamic electrostatic analysis (*25*), and similar techniques (*26*). A previous MCCE (Multi-Conformer Continuum Electrostatics) study of cytochrome *c* oxidase (*27*) determined the E_m and pK_a of the redox centers and key residues in O, E, and R states (*4*).

This work aims to understand the behavior of CcO following the introduction of Asp 44. The redox potential of heme *a* and the pK_a of Asp 44 are calculated and compared with the results for the wild-type protein. The Asp represents a probe of the coupling between electron and proton transfer inside the protein. If the introduced Asp is deprotonated, the free energy of transfer of electrons from Cu_A to heme *a* becomes coupled to Asp protonation changes, introducing new pH dependence to the reaction. The responses of the protein to the addition of a negative charge by reduction of the heme or deprotonation of Asp 44 are compared. The inconsistency of the Asp having a low pK_a while heme oxidation is more favorable than in wild-type CcO is explored.

MATERIALS AND METHODS

Wild-Type and Derivative Structures. Two structures of CcO from *Rb. sphaeroides* are used as input for the calculations: wild-type X-ray structure 2GSM (*28*) with a resolution of 2.0 Å (designated WT_S44) (Table 1) and the S44D mutant X-ray crystal structure provided by the Ferguson-Miller group (Michigan State University, East Lansing, MI) (*12*) (designated Mut_D44). Both wild-type and mutant structures were relaxed with GROMACS (*29*) as described below to yield WT*_D44 and Mut*_D44, respectively (with the asterisk indicating it is a product of GROMACS optimization). Ser 44 in WT_S44 was replaced with an ionized Asp and the resultant structure relaxed with GROMACS to yield WT*_D44. In addition, Asp 44 in WT*_D44 and Mut*_D44 was changed to Ser via MCCE to yield WT*_S44 and Mut*_S44, respectively, without additional GROMACS backbone changes. In all cases, MCCE further relaxes the structure by allowing selection of different side chain positions (*30*). In addition to the mutation site of residue 44 in chain A, there are 12 surface residues that are not seen in the mutant crystal structure and are labeled as Ala. MCCE rotamer packing was used to recover the 2GSM wild-type sequence, yielding structures Mut*_S44# and Mut*_D44#, respectively (the number sign indicating recovery of the 12 surface residues). Overall, there

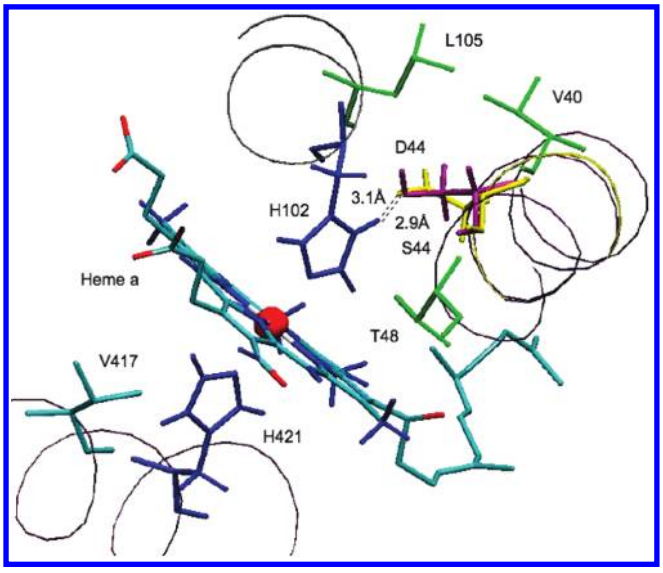

FIGURE 1: Comparison of the region around heme *a* in PDB entry 2GSM (WT_S44) and WT*_D44. Heme *a* and its two distal ligands are shown. Ser 44 and the original backbone are colored purple. Asp 44 and the nearby backbone after GROMACS minimization are colored yellow. Nearby residues Val 40, Leu 105, and Thr 48 (colored green) change position slightly. His 102 is 2.9 Å from Ser 44 in WT_S44. The Asp−His H-bond distance is 3.1 Å in WT*_D44 after GROMACS minimization.

are seven structures used in this study, including four structures with Ser 44 (WT_S44, WT*_S44, Mut*_S44, and Mut*_S44#) and three structures with Asp 44 (WT*_D44, Mut*_D44, and Mut*_D44#) (Table 1).

In Silico Mutation of Ser 44 to Asp. Ser is smaller than Asp. If Asp is added to the wild-type 2GSM structure, the Asp 44−His 102 distance is 2.85 Å but the Asp side chain clashes with the backbone of Phe 47 and Met 106. GROMACS molecular dynamics (version 3.3.2) (*29*) is used to relax the structure. Relaxation uses the GROMACS default mode, in vacuum with a short (< 10 ps) trajectory aimed at relaxing van der Waals clashes. Standard ionization states are used so Asp 44 is ionized. No atoms are constrained, and termination occurs when the energy shifts are less than 0.01 kJ/mol. The final backbone rmsd between WT*_D44 and the original 2GSM wild-type structure is 0.14 Å. The backbone in the vicinity of Asp 44 shifts by ≈0.3 Å to accommodate the larger side chain. The hydrogen bond distance between Asp 44 and His 102 is now 3.1 Å (Figure 1). In the X-ray crystal structure of the S44D mutant, the hydrogen bond distance is 2.7 Å. It increases to 2.88 Å after GROMACS minimization.

MCCE Simulation and Analysis. MCCE combines continuum electrostatics and molecular mechanics to calculate the pK_a and electrochemical midpoint potentials (E_m) for amino acids and cofactors, allowing full side chain rotamer sampling on a fixed backbone (*30*, *31*). MCCE version 2.4 has updated non-electrostatic parameters, and entropy and protein surface corrections. Previous simulation results showed the method provides values that agree with experimental redox potentials for hemes and quinones in large membrane proteins (*32*−*35*), with hemes in proteins with experimental E_m values varying by 800 mV (*36*) and with amino acid pK_a values (*30*). In the benchmark pK_a and E_m calculations, 65% of the site values have errors of less than 1 pH unit or 60 mV, and 92% less than 2 pH units or 120 mV (*30*, *36*).

The four key cofactors, Cu_A, heme *a*, heme a_3, and Cu_B, and the amino acids that serve as their ligands combined into four complexes as described in earlier MCCE calculations (*27*). An atomic partial charge distribution for Cu_A, with two Cu atoms, and side chains of Cys 252 and 256 and His 217 and 260 of chain B was calculated using the B3LYP method, the LANL2DZ basis set, and the CHELPG algorithm in Gaussian 98 (*37*−*39*). Metal-centered charge sets (*36*, *40*) are used for heme *a* and heme a_3 (*27*). Cu_B is ligated to three His residues (at positions 284, 333, and 334) with a water that can loose a proton to form the Cu_B−hydroxy complex (*27*). Atomic charge sets are provided in the Supporting Information.

(*i*) *Energy of the Hydrogen Bond to the Heme His Ligand*. The DFT package, Jaguar (*41*), is employed to determine how well the shift of the heme E_m by the hydrogen bond to the His ligand is captured by a classical continuum electrostatics program such as MCCE. The difference in the total energy of the separated and combined hydrogen bond acceptor and heme−ligand complex gives the hydrogen bond energy (Figure S2 of the Supporting Information). The single point energy of a bis-His−heme model complex (without propionic acids) is calculated with and without an Asp, Asn, or Gly as an acceptor of a hydrogen bond from the His. The classical electrostatics hydrogen bond energy is obtained with Coulomb's law with atomic partial charges derived from each Jaguar calculation. Both Coulomb's law and DFT calculations use a dielectric constant of 6.

Previous studies of the interaction between the dication Cu_B^{2+} and heme a_3, 4.8 Å apart in the binuclear center, showed that very strong interactions can be overestimated in the classical continuum electrostatics calculations (*42*). Cu_B is much closer to heme a_3 in the binuclear complex than the hydrogen bond donor here is to heme *a*. In addition, Cu_B is doubly charged, Ser 44 is neutral, and Asp 44 is singly charged. Good agreement is found between the classical and DFT calculations for the range of interaction energies encountered here. The calculated energy difference in the two methods is less than 0.7 kcal/mol when the H-bond interaction is less than 8 kcal/mol (480 meV). Both the DFT and continuum electrostatics analyses show the energy of the hydrogen bond to the His ligand is stronger in the oxidized Fe(III) than the neutral Fe(II) complex. A neutral hydrogen bond partner shifts the E_m by less than 90 mV, while an optimal interaction with an ionized Asp can lower the E_m by as much as 500 mV, with a dielectric constant of 6. Small differences in hydrogen bond strength are found with the simple metal-centered charge set for the heme used here and the Jaguar-derived NBO charges (Table S4 of the Supporting Information). The NBO charges, which are calculated for each heme−imidazole complex, generally reproduce the DFT energies better than other charge sets. The results support the use of the continuum electrostatics energy to obtain the shift in heme *a* E_m that occurs when the hydrogen bond to the axial heme ligand is changed.

(*ii*) *MCCE Analysis of the E_m of Heme a*. A 35 Å slab of low-dielectric constant material is added with IPECE (*34*) to simulate the membrane low-dielectric environment. DelPhi (*43*−*45*) is used within MCCE to solve the Poisson−Boltzmann equation with an internal dielectric constant for the protein and membrane of 4 and 80 for the solvent. The external salt concentration is 150 mM. Reference redox potentials in water are 264 mV for the Cu_A complex (*46*), −60 mV for the heme *a*−bis-His complex (*47*), and −120 for the heme a_3−aquo-His complex (*9*). PARSE (*48*) charges and radii are used for the amino acids, and the AMBER (*49*) force field is used for torsion and Lennard-Jones parameters. The interaction between heme a_3 and Cu_B is corrected as described in ref *42*. The pK_{sol} used for Asp in MCCE is 4.75, the value for a carboxylate side chain. The measured Asp p$K_{a,sol}$ is lowered in a tripeptide to 3.8 because the

Table 2: Energy Terms Contributing to the E_m Shift of Heme *a* and pK_a Shift of Asp 44[a]

				ΔG_{ele}^{mfe}			fraction charge of D44$^-$ at pH 7	
structure	E_m	$\Delta\Delta G_{rxn}$	$\Delta\Delta G_{pol}$	Asp 44	others	$E_{m,sol}$	ox	mid
WT_S44	378	362	177		*−101*	−60		
WT*_S44	387	363	189		*−105*	−60		
Mut*_S44	375	374	177		*−120*	−60		
Mut*_S44#	372	373	180		*−119*	−60		
avg_S44	378 ± 6	368 ± 6	181 ± 6		−111 ± 10			
WT*_D44	345	363	189	*−34*	*−113*	−60	0.45	0.18
Mut*_D44	329	374	180	*−85*	*−87*	−60	0.85	0.33
Mut*_D44#	318	373	182	*−117*	*−94*	−60	0.88	0.37
avg_D44	331 ± 14	370 ± 6	184 ± 5	*−78 ± 41*	*−98 ± 13*			
diff D44-S44	−47	2	3	*−78*	*13*			

Asp 44	pK	$\Delta\Delta G_{rxn}$	$\Delta\Delta G_{pol}$	heme *a*	others	pK_{sol}
			With Heme Oxidized			
WT*_D44	7.2	600	−97	−392	34	4.75
Mut*_D44	7.3	630	−65	−482	58	4.75
Mut*_D44#	7.0	628	−48	−539	53	4.75
avg	7.2 ± 0.1	619 ± 17	−70 ± 25	−471 ± 74	48 ± 13	4.75
			With Heme Reduced			
WT*_D44	15.2	600	−97	−127	26	4.75
Mut*_D44	17.8	630	−65	−173	17	4.75
Mut*_D44#	17.9	628	−49	−199	57	4.75
avg	17.0 ± 1.5	619 ± 17	−70 ± 24	−166 ± 36	33 ± 21	4.75
diff D44-S44	9.8	0	0	−305	15	

[a]Analysis of the redox potential (E_m) of heme *a* at pH 7 (top section). Analysis of the pK_a of D44 in the presence of the oxidized or reduced heme *a* (bottom section). Structures are defined in Table 1. $E_{m,sol}$ is the reference E_m of heme *a* in aqueous solution. p$K_{a,sol}$ is the pK_a of the Asp carboxylate side chain in solution. $\Delta\Delta G_{rxn}$ is the difference in the desolvation energy of the reactant and product. $\Delta\Delta G_{pol}$ is the difference in the electrostatic and non-electrostatic interaction of product and reactant states with the backbone. ΔG_{ele}^{mfe} is the mean field energy difference of the electrostatic pairwise and van der Waals interactions with the residues in the protein in the reactant and product. The oxidized heme *a* and deprotonated Asp are the product states. See eqs 1 and 2 for a more complete description of terms. pK_{sol} and pK_a are in pH units; the E_m is in millivolts, and all energies are in milli-electron volts. The energy needed to change a pK_a value by 1 pH unit at 25 °C is 58 meV or 5.7 kJ/mol.

neighboring amide backbone dipoles must point their positive end toward the side chain with the larger carbonyl pointing away (*50*). The interaction of the Asp with its neighboring amides is counted explicitly in the MCCE calculations, so using the higher carboxylic acid p$K_{a,sol}$ prevents double counting of the interaction with the backbone. MCCE studies show on average, benchmark Asp pK_as are ≈0.4 pH units too low using the p$K_{a,sol}$ of 4.75 (*30*). They would be expected to be ≈1 pH unit too high if 3.8 were the more appropriate p$K_{a,sol}$.

Given the Boltzmann distribution of side chain and ligand positions and charge generated by Monte Carlo sampling as a function of pH and E_h, the energy terms that determine the E_m of a redox cofactor can be decomposed as (*51*)

$$nFE_m^{mfe} = nFE_{m,sol} + \Delta\Delta G_{rxn} + \Delta G_{bkn} + \Delta G_{res}^{mfe} \quad (1)$$

where $E_{m,sol}$ is the E_m in aqueous solution (*52*), $\Delta\Delta G_{rxn}$ is the desolvation energy penalty moving the cofactor from water into protein, $\Delta\Delta G_{bkn}$ is the electrostatic and nonelectrostatic interaction of the cofactor with the protein backbone, and ΔG_{res}^{mfe} is the mean field pairwise interaction between the cofactor and residues in the protein in the distribution derived by Monte Carlo sampling. In each case, the difference in interaction with the oxidized group and the reduced group is given. ΔG_{res}^{mfe} provides the mean-field approximation for the conformer pairwise interactions, calculated as described in ref *27*, while the full microstate energies are used in the Monte Carlo sampling. The reorganization energy due to conformational or protonation changes coupled to the redox reaction creates small differences between the calculated E_m and the E_m^{mfe} (*31*). A similar equation can be used to explore the factors leading to the shift in Asp pK_a in the protein.

The pK_7' is the effective pK_a for the residue when the ionization and conformation of the rest of the protein are fixed in their Boltzmann distribution found at pH 7 (*27*):

$$pK_7' = pK_{sol} + \Delta\Delta G_{rxn} + \Delta G_{pol} + \Delta G_{res}^{mfe} \quad (2)$$

The pK_a and pK_7' will be different because of changes in the charge of the rest of the protein moving from pH 7 to the pH of the true pK_a.

RESULTS AND DISCUSSION

The side chain of Ser 44 makes a hydrogen bond to His 102, an axial ligand to heme *a* in CcO from *Rb. sphaeroides*. A Gly at the aligned position in the sequence makes the hydrogen bond in bovine CcO (all residues are in subunit I with *Rb. sphaeroides* numbering unless noted). Replacing Ser 44 with Asp allows exploration of what happens when heme *a* reduction becomes strongly coupled to the import of a proton into a buried residue (*12*). This mutation also tests the ability of this protein to accommodate a new charge (*21*). The calculations were conducted with structures derived from the 2GSM wild-type protein and from a structure of the S44D mutant (personal communication with S. Ferguson-Miller). Four structures with a Ser and three with an Asp at position 44 were prepared from these two structures (Table 1). All numbers in the text represent averages of the calculations of the proteins with Ser or with Asp unless otherwise stated. The results with individual structures are listed in Table 2. The change in outcome with different

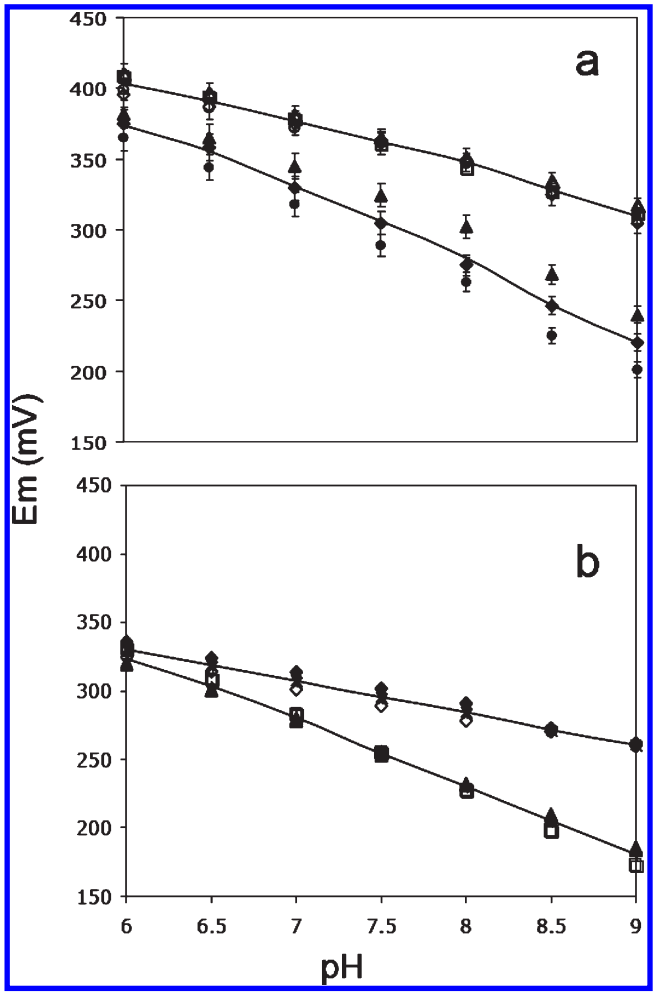

FIGURE 2: pH dependence of (a) heme *a* and (b) Cu_a E_m values. Structures with Ser 44: WT_S44 (□), WT*_S44 (△), Mut*_S44 (◇), and Mut*_S44# (○). Structures with Asp 44: WT*_D44 (▲), Mut*_D44 (◆), and Mut*_D44# (●). The lines connect the average E_m values for all structures with S44 or D44.

structures provides one estimate of the variability of the calculations. The fact that reproducible values are found with the structure of the mutated protein and with the Asp imposed on the wild-type structure indicates that the changes seen here can be assigned to the Asp itself and not to other diffuse changes in the mutated protein structure.

E_m of Heme a at pH 7. The measured heme *a* E_m in *Rb. sphaeroides* CcO is ≈330 mV, similar to the bovine enzyme E_m of 340 mV (*53*, *54*). Analysis of *Rb. sphaeroides* structure 1M56 with an earlier version of MCCE yielded a value of 360 mV (*27*). The redox potential of heme *a* here is calculated in the wild-type Ser 44 and Asp 44 mutant structures using MCCE2.4 with the other three redox centers (Cu_A, Cu_B, and heme a_3) fixed in their oxidized state. This parallels the conditions of the electron transfer measurements, where electron transfer from Cu_A to heme a is determined in the oxidized protein by flash activation of a ruthenium-labeled cytochrome *c* electron donor (*12*). The calculated E_m at pH 7 for heme *a* in the Ser 44 structures is 379 ± 7 mV, in good agreement with experimental measurements and previous MCCE studies. The values found with the initial WT_S44 structure, the structure derived from the mutant X-ray structure (Mut*_S44), and the wild-type structure first relaxed around Asp 44 in GROMACS and than mutated back to Ser 44 (WT*_S44) differ by only 10 mV (Table 2 and Figure 2).

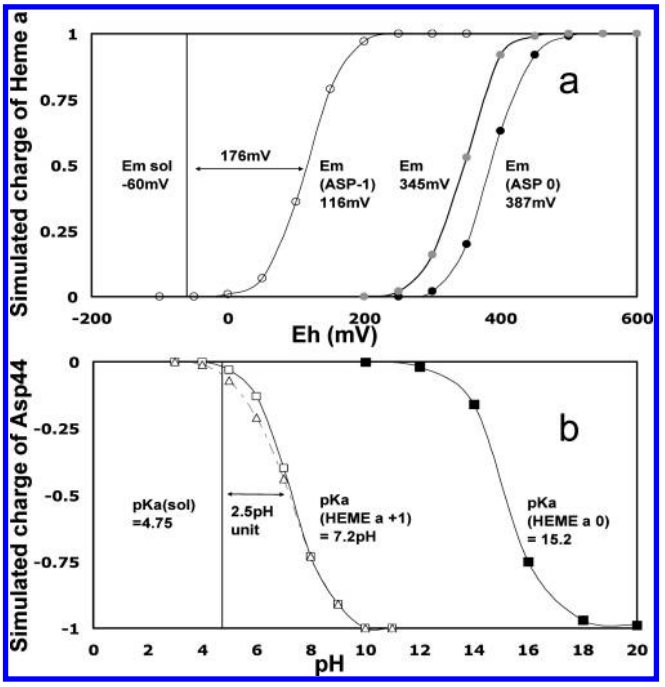

FIGURE 3: (a) Heme *a* E_m titration curve when D44 is fixed to be neutral (●) or ionized (○) or allowed to remain at equilibrium with the heme at pH 7 (gray circles). The redox potential of the heme *a* E_m in solution of −60 mV is shown. (b) The D44 pK_a titration when heme *a* is fixed to be reduced (■) or oxidized (charge of +1) (□ for Mut*_D44 and △ for WT*_D44). The Asp carboxylic acid side chain solution pK_a of 4.75 is shown.

The E_m of heme *a* in the Asp 44 structures is 50 ± 15 mV lower than that with Ser 44 at pH 7 (Table 2 and Figure 2). The E_m was analyzed to determine what energy terms are modified in the mutant protein (eq 1). Heme *a* in both wild-type and mutant structures has essentially the same desolvation energy and interactions with the backbone. It is the partially ionized Asp, which is calculated to have a pK_a near 7, that stabilizes the charge on the heme, decreasing the E_m. If the Asp is fixed in the protonated state, the heme *a* redox potential is 374 mV, negligibly different from 378 mV with the native Ser. The similarity of the E_m with a protonated Asp or with Ser is consistent with experimental findings that an oxidase with an Asn at position 44 behaves very much like the wild-type protein (*12*). The neutral Asp and the Asn have a similar shape and distribution of charges. However, when the Asp is fixed in its deprotonated state with a charge of −1, the heme *a* redox potential decreases from 116 mV (WT*_D44) to 61 mV (Mut*_D44), providing a lower limit for the E_m in the mutant (Table 2 and Figure 3).

pK_a of Asp 44 in the Mutated Structures. The newly introduced Asp can be compared with the 17 Asp residues found in the native CcO. Ten are deeply buried, as defined as having lost at least 6.8 kcal/mol of solvation energy, sufficient to shift the pK_a by 5 pH units in the absence of other interactions with the protein (*19*). Of these buried Asp residues, five are calculated to be fully ionized at pH 5 and only three are not mostly ionized at pH 7. This indicates that the protein "pays back" the stabilization of the ionized Asp by water lost within the protein through interactions with charged and dipolar groups in the protein.

The Asp 44 pK_a is calculated to be ≈7 with heme *a* oxidized in all structures. Thus, the newly introduced charge remains significantly ionized at neutral pH. The energy breakdown shows the expected, large desolvation penalty for this buried Asp, shifting the pK_a up, while the electrostatics pairwise interaction

between the Asp and positively charged heme *a* shifts the pK_a down (eq 2 and Table S1 of the Supporting Information). Interactions with the backbone stabilize the deprotonated Asp, while interactions with other side chains favor the protonated state. The Asp makes a hydrogen bond to His 102, the ligand to heme *a*. The distance varies from 2.86 to 3.10 Å in the different structures (Table 1). At pH 7, the His stabilizes Asp ionization by −34 meV in the structures derived from 2GSM (WT*_D44) and −85 mV in the structures derived from the mutant X-ray structure in which the Asp−His hydrogen bond is shorter (Mut*_D44). The more favorable interaction also leads to an increase in the fraction of Asp ionized and lower heme *a* E_m when the Asp is forced to be ionized (Table S1 of the Supporting Information). The oxidized heme stabilizes the deprotonated Asp by 240−280 meV (Table S1 of the Supporting Information). When the heme *a* is reduced, the Asp pK_a always shifts to be > 15 (Figure 3 and Table S2 of the Supporting Information).

Comparison of E_m and pK_a Shifts in the Protein. The E_m of a bis-His *a*-type heme is −60 mV in solution (*52*), while it is calculated to be 380 mV in the wild-type protein, a shift of 320 meV destabilizing the oxidized heme. In the presence of the ionized Asp, the E_m shifts to 116 mV (WT*_D44 structure). With heme *a* oxidized, the side chain pK_a shifts from 3.8 for an Asp in solution to 7.2 in the protein (Figure 3). This represents a 144 meV destabilization of the charge on the Asp. The mean field energy analysis of the MCCE Monte Carlo conformer population can compare the factors that shift the ionization free energy of heme *a* and Asp 44 (Table 2 and eq 2). The heme, with its larger radius, has a much smaller desolvation penalty than the Asp (*55*), while the backbone favors Asp ionization, due to the overall positive backbone potential within all proteins (*50*). The interactions with the other residues are more favorable for heme *a* than for the Asp. The mutual interaction between the ionized Asp and heme stabilizes each charge by ≈250 meV. As the heme E_m is dependent on the Asp charge, the Asp pK_a is dependent on the heme ionization state. The pK_7' is 7.2 with the heme oxidized and 11.8 with the heme reduced (Table S1 of the Supporting Information and eq 2). This value represents the cost of protonating the Asp at pH 7. It is lower than the true pK_a of 15−18 (Table 2) because the protein as a whole is more negative at the higher pH. Thus, in these calculations at pH 7, the Asp is 40% ionized when the heme is oxidized and is fully protonated when the heme is reduced. The resultant E_m of heme *a* is 345 mV when the titration is free to be coupled to Asp 44 protonation.

The experimental pK_a of Asp 44 is estimated to be close to 5.5 (*27*) when the heme is oxidized, while it is calculated to be ≈7.2 here. There are a variety of sources of error that could be responsible for the higher pK_a. The results rely on the ability of continuum electrostatics to calculate how a group making a hydrogen bond to the axial ligand interacts with the heme (*27*). The interactions of a number of hydrogen bond acceptors from an axial ligand in a bis-His−heme complex were calculated with DFT using Jaguar (*41*). There results were compared with those derived with Coulomb's law, the simplification of the Poisson−Boltzmann analysis used in MCCE, which is valid for a uniform dielectric constant. The classical electrostatics treatment models the heme E_m shifts quite well, so it is unlikely to be a source of the error in the Asp pK_a (see the Supporting Information). Thus, these calculations suggest that the hydrogen bond donor to the His changes the heme E_m via through-space, electrostatic interactions rather than by modifying the interaction of the His ligand with the heme.

The GROMACS minimization is conducted with the Asp ionized, which will tend to pull the structure to stabilize this state lowering the pK_a. However, the crystal structure is made with heme *a* reduced and will therefore have a neutral Asp 44. Mutating the Ser in the wild-type structure to Asp also starts with a protein equilibrated around a neutral group. X-ray structures with the oxidized heme and ionized Asp show the Asp is very disordered (personal communication with S. Ferguson-Miller) and may be able to sample positions that are not available here. The optimized Asp−His hydrogen bond is slightly longer than that found in the X-ray structure. The shorter bond does strengthen the Asp−His interaction. However, comparing the Mut*_D44# structure with a hydrogen bond of 2.86 Å with the Wt*_D44 structure with a 3.10 Å distance shows the pK_a actually increases only from 7.0 to 7.2 as the bond is lengthened. Thus, the pK_a is weakly dependent on the Asp−His distance. Lastly, preliminary calculations of the pK_a values of newly introduced acidic and basic residues into the interior of *Staphylococcal* nuclease (*27*) show that MCCE can overestimate the desolvation penalty of a charge introduced into a site in the protein interior by mutation, increasing the pK_a of introduced acidic residues. The problem appears to be that the analysis underestimates protein relaxation around the novel charge especially when the protein is given a low dielectric constant of 4 as done here. Calculation with a higher dielectric constant would be expected to lower the Asp pK_a.

pH Dependence of the Heme a E_m. The calculated pH dependence of the heme *a* E_m in the Ser 44 structures is 34 mV/pH unit as derived from the slope of the linear regression line from pH 6 to 9. Earlier MCCE calculations also found a pH dependence of ≈30 mV/pH unit (*27*). A range of values from ≈10 (*53*) to 30 (*56*) mV/pH unit have been found in bovine CcO. When Ser 44 is replaced with an Asp, the pH dependence of heme *a* increases to ≈50 mV/pH unit (Figure 2 a).

E_m of Cu_A. The E_m of Cu_A was calculated as a function of pH. The redox potential of Cu_A and its pH dependence are independent of the residue at position 44. This is consistent with the electron transfer kinetics of Cu_A reduction by cytochrome *c* being unaffected by the mutation (*12*). However, the results are sensitive to which initial X-ray structure is the basis of the calculations. The E_m is 320 mV in the 2GSM structures at pH 7, ≈30 mV more negative than in the structures derived from the mutant CcO structure. The difference arises from small changes in relatively distant surface residues of chain B. These residues are farther from the other three redox active centers and so do not affect their E_m values significantly.

The pH dependence of the Cu_A E_m is ≈24 mV/pH unit in the 2GSM-derived structures and ≈45 mV/pH unit in the structures derived from the mutated protein X-ray structure (Figure 2b). Earlier MCCE calculations, using the 1M56 structure of *Rb. sphaeroides* CcO, also yielded a pH dependence of 30 mV/pH unit (*27*). In bovine CcO, measurements show a smaller pH dependence of < 10 mV/pH unit for the Cu_A E_m (from pH 7.0 to 8.1) (*53*, *57*). The $\Delta G°$ for the transfer of electrons from CuA to heme *a* is obtained from $-nF(E_{m,Cu_A} - E_{m,heme})$ (Figure 4). In the analysis of the transfer of electrons from Cu_A to heme *a*, the E_{m,Cu_A} is always taken from the Mut*_S44 structure that has the smallest Cu_A pH dependence, while $E_{m,heme}$ values were compared for the seven different structures (Figure 2a).

Free Energy of the Transfer of Electrons from Cu_A to Heme a. At pH 7, the average $\Delta G°$ in the Ser 44 structures is −75 meV. This is in reasonable agreement with the experimental value of −40 meV in the *Rb. sphaeroides* protein (*14*). The $\Delta G°$ is

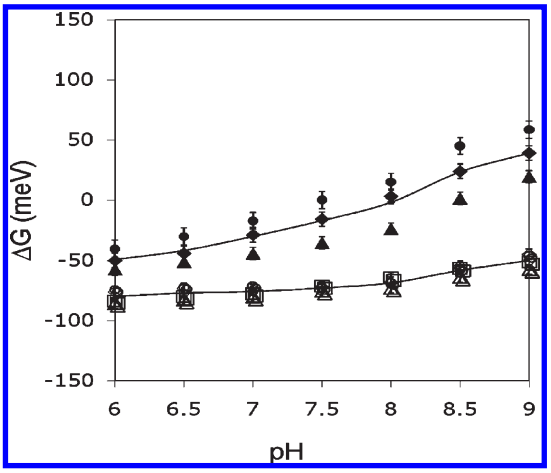

FIGURE 4: Free energy difference between heme *a* and Cu_A as a function of pH. The $\Delta G°$ for the transfer of electrons from Cu_A to heme *a* is obtained from $-nF(E_{m,Cu_A} - E_{m,heme})$. The E_{m,Cu_A} is that found for the Mut*_S44 structure (Figure 2b), while $E_{m,heme}$ values were compared for the seven different structures (Figure 2a). Symbols are as found in Figure 2.

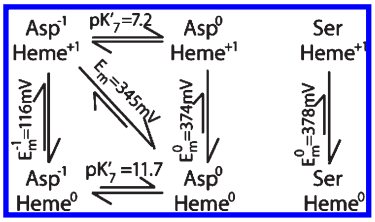

FIGURE 5: Comparison of heme *a* reduction with Ser 44 and Asp 44. $E_m°$ is the heme *a* redox potential for wild-type CcO with Ser 44 or for the WT*_D44 protein when Asp is fixed in its neutral, protonated state. E_m^{-1} is the redox potential when Asp 44 is fixed in its ionized state. E_m is calculated in the Asp 44 protein when Asp ionization is kept at equilibrium with the pH and heme redox state. In these calculations at pH 7, the Asp is partially ionized when the heme is oxidized. Heme ionization is coupled to proton uptake so that the Asp is fully protonated when heme *a* is reduced. Data are from WT_S44 and WT*_D44 calculations.

−30 meV in the Asp 44 mutant, while the experimental value is −60 meV (*12*). While the calculated $\Delta G°$ for the mutant is consistent with the measured value given the error range of the calculations, the change upon moving from the wild-type to mutated protein is not.

A thermodynamic analysis (Figure 5) shows that the driving force for the transfer of electrons from Cu_A to heme *a* should be less favorable when the starting state is Asp 44^-heme^{ox} since Asp proton binding adds a cost to the heme *a* reduction. This assumes the E_m of Cu_A is the same if the Asp is ionized or protonated and that the heme *a* E_m is similar with Ser 44 or a protonated Asp 44 (Figure 4). These conditions are supported by these calculations and by earlier experiments (*12*). The shift in heme *a* E_m is only 45 meV here because the calculated Asp pK_a in the mutant is ≈7 so the cost to protonate it at pH 7 is small. If the Asp pK_a were 5.5 as found experimentally, the driving force for heme *a* reduction would be 90 meV less favorable because Asp^- is more stable and so stabilizes the starting state. The transfer of electrons from Cu_A to heme *a* would now be uphill. The fact that experimentally the reduced heme *a* is more stable than in the wild-type protein, while the Asp pK_a is so low, reveals that there must be additional factors stabilizing the AspH:heme a^{red} species that are not captured here.

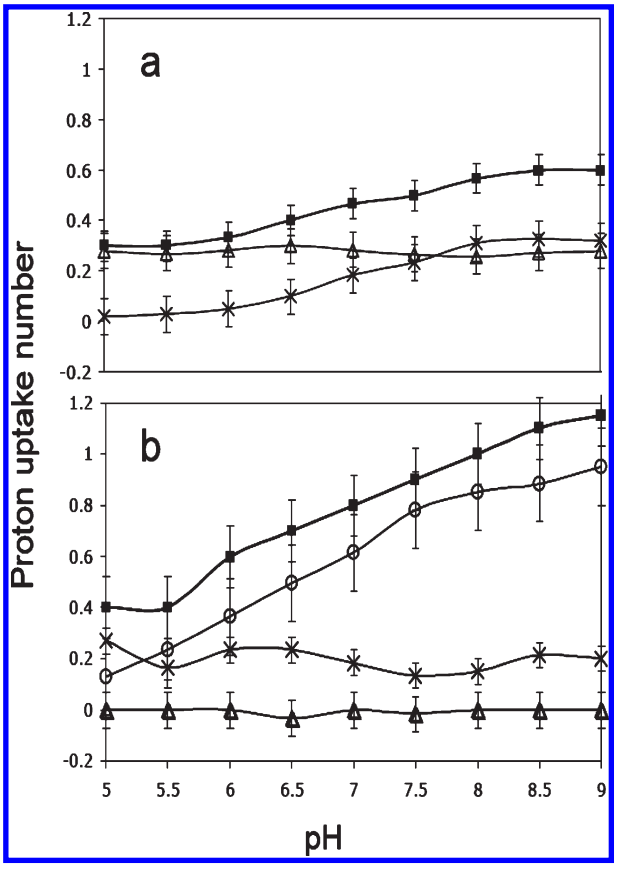

FIGURE 6: pH-dependent proton uptake when heme *a* is reduced in (a) S44 and (b) D44 structures: (■) total proton uptake, (×) uptake for the His 93 and Glu 182 pair, (△) uptake for the rest of the protein, and (○) uptake for Asp 44.

Response of the Protein to Deprotonation of Asp 44 or Reduction of Heme a. The uptake of protons from the protein that accompanies heme *a* reduction with the other cofactors held oxidized was assessed (Figure 6). There are 0.5 proton taken up from solution at pH 7 when heme *a* is reduced in the Ser 44 structures (Figure 6 and the Supporting Information). This increases to 0.6−0.7 at pH 9. As has been seen in earlier MCCE calculations (*27*), His 93 and Glu 182, whose protonation is coupled together, are the most important proton acceptors in the Ser 44 structures. Increasing the pH to 9 increases the total proton uptake by 0.2 proton bound to the H93/E182 cluster.

With the addition of Asp 44, when the ionization of Asp 44 remains in equilibrium with the heme redox state, 0.75 proton is taken up when heme *a* is reduced at pH 7. It increases to 1.15 at pH 9 where Asp 44 is fully ionized in the oxidized heme initial state. The uptake is mostly to Asp 44, while now none is to His 93 or Glu 182 (Figure 6b). No other residue undergoes a significant change in proton uptake with pH. One goal of these calculations is to identify potential donors of protons to the Asp. However, the nearest ionizable residues that contribute small amounts to proton uptake (< 0.05 H^+/e^-) are Arg 52, 481, and 482, which are 12−13 Å away. Other residues > 20 Å away show protonation shifts at the limits of the MCCE sampling noise of ≈0.02. As the sites that respond to the change in charge at Asp 44 and heme *a* are relatively far away, the protonation shifts throughout the protein are the same when the Asp loses a proton when the heme remains reduced or when the oxidized heme is reduced with Asp fixed in its protonated form. In each case, the charge on the Asp 44:heme structure changes from 0 to −1, and in either case, the

rest of the protein binds 0.3 proton to keep a net change in charge of −0.7 (Supporting Information). When the Asp is deprotonated, the protein as a whole loses 0.7 proton. When the heme is reduced, the protein binds 0.3 proton. Thus, the protein is behaving as a buffer, reducing the effect of the change in charge in and around heme *a* by small changes distributed throughout the protein (*1*).

It has been suggested that an internal site donates the proton required for heme *a* reduction to Asp 44 (*12*). This requires a residue or group of residues that is protonated in the Asp^{-}:$heme^{ox}$ state and deprotonated in the AspH:$heme^{red}$ state. Deprotonating the Asp with the heme held oxidized at pH 7 changes the net charge of the protein by only −0.2. Thus, 0.8 proton is distributed to the ensemble average protonation of other residues throughout the protein. However, all of these sites are quite far from the Asp, and no individual residue is found whose equilibrium protonation is strongly coupled to that of Asp 44.

The Low-Energy Pathway for Proton-Coupled Heme a Reduction in the Presence of Asp 44. The experimental study of the Asp 44 CcO and the calculations reported here support the view that an Asp is significantly deprotonated at neutral pH when heme *a* is oxidized and fully protonated when the heme is reduced at pH 7. Long-range electron transfer from Cu_A is now coupled to proton uptake. The rate of proton-coupled electron transfer increases from 10 to 130 s^{-1}, while it is ≈90000 s^{-1} in the wild-type protein (*12*), a decrease of ≈10^3−10^4-fold. The reaction cannot be truly concerted (the diagonal path in Figure 5) as the protons and electrons come from different donors. Rather, it will follow one of the two paths around Figure 5, either first protonating Asp 44 (forming AspH:$heme^{ox}$) or reducing heme (Asp^{-1}:$heme^{red}$) (*58*). The calculations provide an estimate of the relative energy of the two possible intermediates. Assuming Cu_A is the electron donor, the reaction through the Asp^{-1}:$heme^{red}$ state is 200 meV uphill. Thus, at room temperature, the electron first pathway goes through an intermediate that will be present in a ratio with the ground state of 1:2000. Electron transfer could thermally populate the Asp^{-1}:$heme^{red}$ state by a fast but unfavorable electron transfer (*59*, *60*). This would slow the rate 2000-fold even if the transfer of the electron from Cu_A is unchanged and proton uptake not rate-limiting. However, though this intermediate is certainly sufficiently low in energy to be thermally accessible, a proton must still be bound to the Asp to generate a stable product.

The proton first pathway via the AspH:$heme^{ox}$ state has an energy cost close to 0 meV given the Asp 44 pK_7' of 7.2 or 100 meV uphill if the pK_a is 5.5 as found experimentally. Thus, this path is energetically favored. The Asp is deeply buried and not connected to the surface by any of the evolved proton pathways. Within 5 Å of the Asp are Ala 46, Gly 41, Ile 43, Leu 42 and 105, Met 106, Phe 47, Thr 48, and Val 40 and 45. These provide no easy pathway for the transfer of protons to Asp 44. In addition, in these structures, there are no cavities that could hold a water near the Asp. Without some distortion of the structure, delivery of a proton to the Asp could be quite slow.

CONCLUDING REMARKS

These calculations highlight a number of aspects of the behavior of the S44D CcO mutant (*12*). Here an Asp is introduced into a region where there are no polar groups except one Thr and the His from which the Asp will accept a hydrogen bond. There are no cavities large enough to hold a water in the available X-ray crystal structures. Added buried acidic or basic residues are often found to have significant pK_a shifts to stabilize the neutral form of the residue and significantly destabilize the protein when the mutated site is ionized (*21*). However, here the Asp remarkably retains a fairly low pK_a if heme *a* is oxidized, and the wealth of experiments conducted with the mutant shows the protein remains functional in the Asp^{-}:$heme^{ox}$ state. The interaction with the oxidized heme lowers the pK_a by 5.5 pH units (Figure 5). The stability of the protein hosting the Asp can be explained given that the net charge on the protein with the ionized Asp (Asp^{-}:$heme^{ox}$) is the same as that of the native protein with a reduced heme *a* (Ser:$heme^{red}$) (Figure S1 of the Supporting Information). Thus, this anionic mutation is stabilized by the factors that support heme *a* reduction.

The calculations are dependent on the interaction between the oxidized heme *a* and Asp 44, the acceptor of the hydrogen bond from the His ligand. A hydrogen bond of this kind is found in 75% of *b*- and *c*-type hemes collected in a nonredundant database (*10*). The similarity of the shift in the heme E_m calculated in a model complex with density functional theory and with Coulomb's law shows the Asp interacts with the heme in a manner that can be treated as a through-space interaction (pages 9−12 of the Supporting Information).

The calculated pK_a of the Asp is ≈1.5 pH units higher than the measured value. MCCE analysis of benchmark pK_a values reported 84% of the errors are <1.5 pH units (*30*). The fact that all structures used here were obtained with a neutral Asp will tend to increase the pK_a. The analysis is still able to account for much of the stability of the ionized Asp, which has lost ≈14 kcal/mol of the energy that would stabilize an ionized Asp in water because of its position deep in the protein. This desolvation penalty would increase the pK_a by more than 10 pH units in the absence of favorable interactions with the protein. The nearby oxidized heme *a* is the most important factor stabilizing the deprotonated Asp, while the backbone dipoles and the hydrogen bond to the His also lower the pK_a.

The analysis reveals an inconsistency in the model that has been derived from the experimental data. This combines a pK_a for Asp 44 of <7, obligatory protonation of the Asp when the heme is reduced, and a more favorable transfer of electrons from Cu_A to heme, while the Cu_A electrochemistry is unaffected by the residue at position 44 (*12*). The thermodynamic analysis of the coupled electron transfer shows that a low Asp 44 pK_a stabilizes the $Asp\ 44^{-}$:$heme^{ox}$ state. This will make the Asp 44H:$heme^{red}$ state less favorable. The additional factors stabilizing the reduced heme in the mutated protein remain unknown.

ACKNOWLEDGMENT

We are grateful to Ling Qin and Shelagh Ferguson-Miller (Michigan State University, East Lansing, MI) for providing the coordinates for the S44D X-ray crystal structure prior to publication and Christian Fufezan for his work on the analysis of the hydrogen bonds to the heme ligands in his nonredundant heme protein database. We thank Dr. Yifan Song and Jianxun Lu for helpful discussion.

SUPPORTING INFORMATION AVAILABLE

The energy breakdown that leads to the calculated Asp pK_a and pK_7' while heme *a* is fixed in the oxidized state and reduced

state are presented in Tables S1 and S2. The atomic charge sets used in the MCCE calculation are listed in Table S3. Figure S1 gives the total protein proton uptake as a function of the total charge of Asp 44 (or Ser 44) with heme *a*. The change in the E_m of a bis-His−heme model complex due to the presence of a hydrogen bond acceptor from one of the His ligands calculated with DFT or continuum electrostatics continuum electrostatics is given (pages 9−12). This material is available free of charge via the Internet at http://pubs.acs.org.

REFERENCES

1. Rich, P. R. (1995) Towards an understanding of the chemistry of oxygen reduction and proton translocation in the iron-copper respiratory oxidases. *Aust. J. Plant Physiol. 22*, 479–486.
2. Michel, H. (1999) Cytochrome c oxidase: Catalytic cycle and mechanisms of proton pumping-A discussion. *Biochemistry 38*, 15129–15140.
3. Verkhovsky, M. I., Belevich, I., Bloch, D. A., and Wikström, M. (2006) Elementary steps of proton translocation in the catalytic cycle of cytochrome oxidase. *Biochim. Biophys. Acta 1757*, 401–407.
4. Brzezinski, P., and Larsson, G. (2003) Redox-driven proton pumping by heme-copper oxidases. *Biochim. Biophys. Acta 1605*, 1–13.
5. Mitchell, R., Mitchell, P., and Rich, P. R. (1992) Protonation states of the catalytic intermediates of cytochrome c oxidase. *Biochim. Biophys. Acta 1101*, 188–191.
6. Babcock, G. T., and Wikström, M. (1992) Oxygen activation and the conservation of energy in cell respirations. *Nature 356*, 301–308.
7. Ferguson-Miller, S., and Babcock, G. T. (1996) Heme/copper terminal oxidases. *Chem. Rev. 96*, 2889–2907.
8. Wikström, M. (2004) Cytochrome c oxidase: 25 years of the elusive proton pump. *Biochim. Biophys. Acta 1655*, 241–247.
9. Reedy, C. J., and Gibney, B. R. (2004) Heme protein assemblies. *Chem. Rev. 104*, 617–649.
10. Fufezan, C., Zhang, J., and Gunner, M. R. (2008) Ligand preference and orientation in b- and c-type heme-binding proteins. *Proteins 73*, 690–704.
11. Schneider, R., and Sander, C. (1996) The HSSP database of protein structure-sequence allignments. *Nucleic Acids Res. 24*, 201–205.
12. Mills, D. A., Xu, S., Geren, L., Hiser, C., Qin, L., Sharpe, M. A., McCracken, J., Durham, B., Millett, F., and Ferguson-Miller, S. (2008) Proton-dependent electron transfer from CuA to Heme a and altered EPR spectra in mutants close to Heme a of cytochrome oxidase. *Biochemistry 47*, 11499–11509.
13. Winkler, J. R., Malström, B. G., and Gray, H. B. (1995) Rapid electron injection into multisite metalloproteins: Intramolecular electron transfer in cytochrome oxidase. *Biophys. Chem. 54*, 199–209.
14. Zaslavsky, D., Sadoski, R., Wang, K., Durham, B., Gennis, R., and Millett, F. (1998) Single electron reduction of cytochrome c oxidase compound F: Resolution of partial steps by transient spectroscopy. *Biochemistry 37*, 14910–14916.
15. Farver, O., Grell, E., Ludwig, B., Michel, H., and Pecht, I. (2006) Rates and equilibrium of CuA to heme a electron transfer in *Paracoccus denitrificans* cytochrome *c* oxidase. *Biophys. J. 90*, 2131–2137.
16. Grunwald, E., and Berkowitz, B. J. (1951) The measurement and correlation of acid dissociation constants for carboxylic acids in the system ethanol-water. Activity coefficients and empirical activity functions. *J. Am. Chem. Soc. 73*, 4939–4944.
17. Warshel, A., and Russell, S. T. (1984) Calculations of electrostatic interactions in biological systems and in solutions. *Q. Rev. Biophys. 17*, 283–422.
18. Barrette, W. C., Johnson, H. W., and Sawyer, D. T. (1984) Voltammetric evaluation of the effective acidities (pK_a') for Brønsted acids in aprotic solvents. *Anal. Chem. 56*, 1890–1898.
19. Kim, J., Mao, J., and Gunner, M. R. (2005) Are acidic and basic groups in buried proteins predicted to be ionized? *J. Mol. Biol. 348*, 1283–1298.
20. Bartlett, G. J., Porter, C. T., Borkakoti, N., and Thornton, J. M. (2002) Analysis of catalytic residues in enzyme active sites. *J. Mol. Biol. 324*, 105–211.
21. Isom, D. G., Cannon, B. R., Castaneda, C. A., Robinson, A., and Garcia-Moreno, B. (2008) High tolerance for ionizable residues in the hydrophobic interior of proteins. *Proc. Natl. Acad. Sci. U.S.A. 105*, 17784–17788.
22. Siegbahn, P. E. M., and Blomberg, M. R. A. (2007) Energy diagrams and mechanism for proton pumping in cytochrome c oxidase. *Biochim. Biophys. Acta 1767*, 1143–1156.
23. Ghosh, N., Prat-Resina, X., Gunner, M. R., and Cui, Q. (2009) Microscopic pK_a analysis of Glu286 in cytochrome c oxidase (*Rhodobacter sphaeroides*): Toward a calibrated molecular model. *Biochemistry 48*, 2468–2485.
24. Xu, J., and Voth, G. (2008) Redox-coupled proton pumping in cytochrome c oxidase: Further insights from computer simulation. *Biochim. Biophys. Acta 1777*, 196–201.
25. Olsson, M. H. M., and Warshel, A. (2006) Monte Carlo simulations of proton pumps: On the working principles of the biological valve that controls proton pumping in cytochrome c oxidase. *Proc. Natl. Acad. Sci. U.S.A. 103*, 6500–6505.
26. Quenneville, J., Popovic, D. M., and Stuchebrukhov, A. A. (2006) Combined DFT and electrostatics study of the proton pumping mechanism in cytochrome c oxidase. *Biochim. Biophys. Acta 1757*, 1035–1046.
27. Song, Y., Michonova-Alexova, E., and Gunner, M. R. (2006) Calculated proton uptake on anaerobic reduction of cytochrome c oxidase: Is the reaction electroneutral? *Biochemistry 45*, 7959–7975.
28. Qin, L., Hiser, C., Mulichak, A., Garavito, R. M., and Ferguson-Miller, S. (2006) Identification of conserved lipid/detergent-binding sites in a high-resolution structure of the membrane protein cytochrome c oxidase. *Proc. Natl. Acad. Sci. U.S.A. 103*, 16117–16122.
29. Van Der Spoel, D., Lindahl, E., Hess, B., Groenhof, G., Mark, A. E., and Berendsen, H. J. (2005) GROMACS: Fast, flexible, and free. *J. Comput. Chem. 26*, 1701–1718.
30. Song, Y., Mao, J., and Gunner, M. R. (2009) MCCE2: Improving protein pK_a calculations with extensive side chain rotamer sampling. *J. Comput. Chem. 30*, 2231–2247.
31. Mao, J., Hauser, K., and Gunner, M. R. (2003) How cytochromes with different folds control heme redox potentials. *Biochemistry 42*, 9829–9840.
32. Lancaster, C. R. D., Michel, H., Honig, B., and Gunner, M. R. (1996) Calculated coupling of electron and proton transfer in the photosynthetic reaction center of *Rhodopseudomonas viridis*. *Biophys. J. 70*, 2469–2492.
33. Alexov, E. G., and Gunner, M. R. (1999) Calculated protein and proton motions coupled to electron transfer: Electron transfer from Q_A^- to Q_B in bacterial photosynthetic reaction centers. *Biochemistry 38*, 8253–8270.
34. Song, Y., Mao, J., and Gunner, M. R. (2003) Calculation of proton transfers in bacteriorhodopsin bR and M intermediates. *Biochemistry 42*, 9875–9888.
35. Zhu, Z., and Gunner, M. R. (2005) Energetics of quinone-dependent electron and proton transfers in *Rhodobacter sphaeroides* photosynthetic reaction centers. *Biochemistry 44*, 82–96.
36. Zheng, Z., and Gunner, M. R. (2009) Analysis of the electrochemistry of hemes with E_ms spanning 800 mV. *Proteins 75*, 719–734.
37. Frisch, M. J., Trucks, G. W., Schlegel, H. B., Scuseria, G. E., Robb, M. A., Cheeseman, J. R., Zakrzewski, V. G., Montgomery, J. A., Jr., Stratmann, R. E., Burant, J. C., Dapprich, S., Millam, J. M., Daniels, A. D., Kudin, K. N., Strain, M. C., Farkas, O., Tomasi, J., Barone, V., Cossi, M., Cammi, R., Mennucci, B., Pomelli, C., Adamo, C., Clifford, S., Ochterski, J., Petersson, G. A., Ayala, P. Y., Cui, Q., Morokuma, K., Malick, D. K., Rabuck, A. D., Raghavachari, K., Foresman, J. B., Cioslowski, J., Ortiz, J. V., Baboul, A. G., Stefanov, B. B., Liu, G., Liashenko, A., Piskorz, P., Komaromi, I., Gomperts, R., Martin, R. L., Fox, D. J., Keith, T., Al-Laham, M. A., Peng, C. Y., Nanayakkara, A., Challacombe, M., Gill, P. M. W., Johnson, B., Chen, W., Wong, M. W., Andres, J. L., Gonzalez, C., Head-Gordon, M., Replogle, E. S., and Pople, J. A. (1998) Gaussian 98, revision A.9, Gaussian, Inc., Pittsburgh, PA.
38. Becke, A. D. (1993) Density-Functional Thermochemistry. 3. The role of exact exchange. *J. Chem. Phys. 98*, 5648–5652.
39. Hay, P. J., and Wadt, W. R. (1985) Ab initio effective core potentials for molecular calculations. Potentials for the transition metal atoms Sc to Hg. *J. Chem. Phys. 82*, 270–283.
40. Gunner, M. R., and Honig, B. (1992) Calculations of proton uptake in *Rhodobacter sphaeroides* reaction centers. In The Photosynthetic Bacterial Reaction Center: Structure, Spectroscopy and Dynamics II (Breton, J., and Vermeglio, A., Eds.) pp 403−410, Plenum, New York.
41. Jaguar 6.5 (2005) Schrodinger, LLC, Portland, OR.
42. Song, Y., Mao, J., and Gunner, M. R. (2006) Electrostatic environment of hemes in proteins: pK_as of hydroxyl ligands. *Biochemistry 45*, 7949–7958.
43. Nicholls, A., and Honig, B. (1991) A rapid finite difference algorithm utilizing successive over-relaxation to solve the Poisson-Boltzmann equation. *J. Comput. Chem. 12*, 435–445.
44. Bharadwaj, R., Windemuth, A., Sridharan, S., Honig, B., and Nicholls, A. (1995) The fast multipole boundary element method

for molecular electrostatics: An optimal approach for large systems. *J. Comput. Chem. 16*, 898–913.
45. Rocchia, W., Alexov, E., and Honig, B. (2001) Extending the applicability of the nonlinear Poisson-Boltzmann equation: Multiple dielectric constants and multivalent ions. *J. Phys. Chem. B 105*, 6507–6514.
46. Ostermeier, C., Iwata, S., and Michel, H. (1996) Cytochrome *c* oxidase. *Curr. Opin. Struct. Biol. 6*, 460–466.
47. Vanderkooi, G., and Stotz, E. (1965) Reductive alteration of Heme a hemochromes. *J. Biol. Chem. 240*, 3418–3424.
48. Sitkoff, D., Sharp, K. A., and Honig, B. (1994) Accurate calculation of hydration free energies using macroscopic solvent models. *J. Phys. Chem. 98*, 1978–1988.
49. Cornell, W. D., Cieplak, P., Bayly, C. I., Gould, I. R., Merz, K. M., Jr., Ferguson, D. M., Spellman, D. C., Fox, T., Caldwell, J. W., and Kollman, P. A. (1995) A second generation force field for the simulation of proteins, nucleic acids, and organic molecules. *J. Am. Chem. Soc. 117*, 5179–5197.
50. Gunner, M. R., Saleh, M. A., Cross, E., ud-Doula, A., and Wise, M. (2000) Backbone dipoles generate positive potentials in all proteins: Origins and implications of the effect. *Biophys. J. 78*, 1126–1144.
51. Gunner, M. R., Mao, J., Song, Y., and Kim, J. (2006) Factors influencing energetics of electron and proton transfers in proteins. What can be learned from calculations. *Biochim. Biophys. Acta 1757*, 942–968.
52. Vanderkooi, G., and Stotz, E. (1966) Oxidation-reduction potentials of Heme a hemochromes. *J. Biol. Chem. 241*, 3316–3323.
53. Moody, A. J., and Rich, P. R. (1990) The effect of pH on redox titrations of Heme a in cyanide liganded cytochrome c oxidase: Experimental and modeling studies. *Biochim. Biophys. Acta 1015*, 205–215.
54. Wang, K., Zhen, Y., Sadoski, R., Grinnell, S., Geren, L., Ferguson-Miller, S., Durham, B., and Millett, F. (1999) Definition of interaction domain for the reaction of cytochrome c with cytochrome c oxidase: II. Rapid kinetics analysis of electron transfer from cytochrome c to *Rhodobactor sphaeroides* cytochrome oxidase surface mutants. *J. Biol. Chem. 274*, 38042–38050.
55. Bockris, J. O. M., and Reddy, A. K. N. (1973) Modern Electrochemistry, Vol. 1, Plenum, New York.
56. Artzatbanov, V. Y., Konstantinov, A. A., and Skulachev, V. P. (1978) Involvement of intramitochondrial protons in redox reactions of cytochrome α. *FEBS Lett. 87*, 180–185.
57. Erecinska, M., Chance, B., and Wilson, D. F. (1971) The oxidation-reduction potential of the copper signal in pigeon heart mitochondria. *FEBS Lett. 16*, 284–286.
58. Graige, M. S., Paddock, M. L., Bruce, J. M., Feher, G., and Okamura, M. Y. (1996) Mechanism of proton-coupled electron transfer for quinone (Q_B) reduction in reaction centers of *Rb. sphaeroides*. *J. Am. Chem. Soc. 118*, 9005–9016.
59. Woodbury, N. W., Parson, W. W., Gunner, M. R., Prince, R. C., and Dutton, P. L. (1986) Radical-pair energetics and decay mechanisms in reaction center containing anthraquinones or benzoquinones in place of ubiquinone. *Biochim. Biophys. Acta 851*, 6–22.
60. Xu, Q., and Gunner, M. R. (2000) Temperature dependence of the free energy, enthalpy and entropy of $P^+Q_A^-$ charge recombination in photosynthetic reaction centers. *J. Phys. Chem. B 104*, 8035–8043.